THE ASTROPHYSICAL JOURNAL, 345:881–893, 1989 October 15

FAR-INFRARED EMISSION IN THE ρ OPHIUCHI REGION: A COMPARISON WITH MOLECULAR GAS EMISSION AND VISUAL EXTINCTION

T. H. JARRETT AND R. L. DICKMAN
Five College Radio Astronomy Observatory and Department of Physics and Astronomy, University of Massachusetts at Amherst
AND
W. HERBST
Department of Astronomy, Van Vleck Observatory, Wesleyan University
Received 1988 October 26; accepted 1989 April 13

ABSTRACT

We present results of a combined *IRAS*, optical and molecular line study of a 40′ × 40′ region near the southeast edge of the ρ Oph molecular cloud. Co-added *IRAS* survey data reveals far-infrared emission from 12 to 100 μm, spread throughout the cloud. The 60 and 100 μm intensities are consistent with thermal emission from interstellar dust at a color temperature a few degrees higher than the mean gas temperature derived from our CO $J = 1$–0 observations. The two temperature estimators are well correlated with each other except near the cloud edge, where clear evidence of subthermal molecular excitation is seen. The dust opacity derived from the 60 and 100 μm intensities is reasonably well correlated with the molecular gas column density and with visual extinction derived from star counts up to $A_v \sim 5$ mag. Beyond this point, the dust opacity shows greatly increased scatter. When areas near strong IR or molecular outflow sources are avoided, however, the 60 μm opacity is found to be fairly well correlated with extinction up to $A_v \geq 10$ mag. These results suggest that the *IRAS* data base can be used to trace the bulk of the Galactic interstellar dust.

In contrast to the longer wavelength IR emission, the 12 and 25 μm emission possesses a color temperature far too high (>200 K) to be attributable to dust in thermal equilibrium with the cloud gas. Further, the opacity associated with this emission shows virtually no correlation with either the long-wavelength IR opacity or A_v.

Subject headings: infrared: sources — interstellar: grains — interstellar: molecules — nebulae: individual (ρ Oph)

I. INTRODUCTION

As anticipated, the *IRAS* satellite revealed diffuse far-infrared continuum radiation emanating from the interstellar medium. In the specific case of cool molecular clouds, the far-infrared spectrum usually peaks near, or beyond, 100 μm, and exhibits a steep falloff shortward of the 60 μm band (see Beichman *et al.* 1984); there is generally little radiation at the *IRAS* short-wavelength bands of 12 and 25 μm, except toward bright point sources. These properties are consistent with thermal emission at a temperature not too different from that inferred from observations of the molecular gas associated with these objects.

Several recent studies have attempted a detailed comparison of the far-infrared radiation revealed by *IRAS* with the molecular line emission from cold, opaque clouds. Boulanger and Perault (1988) compared 100 μm intensity with gas column density in the Orion A and Chamaeleon II dark clouds. For the Chamaeleon clouds, they find a fairly tight linear correlation between the two components for relatively low extinctions ($A_v < 3$). In the case of Orion, the linear trend found for Chamaeleon defines a lower bound for a relation with far more scatter. In Heiles Cloud 2 of the Taurus cloud complex, Cernicharo and Guélin (1987) find a correlation between far-infrared emission, gas column density, and visual extinction, but again the extinctions are not very high. Snell, Heyer, and Schloerb (1989) also studied this region, in addition to B18, another filament in the Taurus complex. They find a tight correlation between dust opacity, and gas column density inferred from ^{13}CO integrated intensity. However, only 2%–5% of the dust mass is apparently responsible for the observed dust emission. Despite this, Snell, Heyer, and Schloerb conclude that even though the bulk of the dust in Taurus is invisible to *IRAS*, what is seen does satisfactorily trace the internal structure of the cloud. Langer *et al.* (1988) find a similar result for the dark cloud Barnard 5, with 100 μm dust opacity following gas column density in spite of the fact that only a fraction of the total dust mass is detected. Green and Young (1989) suggest that a correlation exists between ^{18}CO column density and far-IR dust emission within the central core of the ρ Ophiuchi molecular cloud, but do not make a detailed, point comparison of the two quantities.

With the exception of Green and Young's work, none of the studies cited above examined regions with extinctions in the visible significantly higher than ~5 mag, and it is as yet unclear whether *IRAS* observations of more opaque regions can provide quantitative probes of their structure. A related issue concerns the well-known insensitivity of *IRAS* to dust significantly colder than ~20 K. Owing to the essentially exponential dependence of the infrared emission from such regions, the cold, high-extinction cores of molecular clouds without massive star formation—regions which are expected to be virtually unheated by the interstellar uv radiation field—may be essentially invisible to *IRAS*.

In this paper we compare the dust characteristics of a 40′ × 40′ section of the ρ Ophiuchi molecular cloud complex revealed by the *IRAS* satellite, with both molecular line and

deep star count data for the region. The cloud offers regions of remarkably high dust column density (Wilking and Lada 1983; Dickman and Herbst 1989), as well as gas temperatures roughly twice that of a typical dark cloud (see §§ II*a* and III*b*). The latter issue is important because dust that is thermally coupled to the gas may have a temperature just high enough to be detectable by *IRAS*. The ρ Oph cloud is also unusual in that it is clearly visible at 12 and 25 μm (see § III). Our goals are to evaluate the utility of the *IRAS* data in tracing the internal structure of a relatively warm molecular cloud over a substantially larger extinction range than has been previously studied, and to compare the properties of dust emission in this cloud with those reported in order to clarify the nature of the 12 and 25 μm emission detected by the satellite for other sources.

II. OBSERVATIONS AND DATA ANALYSIS

a) General Background

The ρ Ophiuchi cloud lies in a northern extension of the Scorpius OB2 association at a distance of 160 pc (Bok 1956; Herbst and Warner 1981). The region includes one O star, ζ Oph (O9), lying more than 10° north of ρ Oph, several B stars in close proximity to the cloud, and a red supergiant, Antares, which lies only $\sim 1°$ south of ρ Oph (Herbst and Warner 1981). There is a wealth of observational data for this region, including molecular line emission studies (Myers *et al.* 1978; Lada and Wilking 1980; Loren *et al.* 1980; Wilking and Lada 1983; Loren and Wootten 1986; Wootten and Loren 1987; Loren 1989*a*, *b*) and near-infrared 2 μm photometry studies (Grasdalen, Strom, and Strom 1973; Vrba *et al.* 1975; Elias 1978; Wilking and Lada 1983), primarily because the cloud is regarded as an ideal laboratory for active star formation. Wilking and Lada (1983) estimate the visual extinction toward the core of the ρ Oph cloud to be $A_v = 50$–106 mag, implying a total cloud mass of 550 $M_\odot$ in the 2 pc^2 central region of the cloud. Clearly, this is a region of unusually large column density. The ρ Oph complex is also known for its anomalously high ratio of total to selective extinction, which has been determined by numerous workers to have values exceeding 4 over much of the cloud (Carrasco, Strom, and Strom 1973; Brown and Zuckerman 1975; but also see Elias 1978). It has been suggested that this result indicates an increase in the mean size of dust grains relative to the generally prevalent size in the ISM. Observations of an unusually large wavelength of maximum linear polarization for the grains also supports this conjecture (Draine 1985).

The region studied in this paper is a section of the southeast area of the ρ Oph cloud (coordinates are given below). The region was selected for study because it contains both nearly unobscured as well as extremely opaque areas within a single $\sim 50'$ diameter 4 m prime focus field. Lynds (1962) assigned the southeast filament of the Oph cloud its own catalog number, L1689, which extends into the L1612 and L1629 filaments (Loren 1989*a*), but the molecular data show the filament to be kinematically undifferentiated from the rest of the cloud. Further, like the bulk of the parent cloud itself, the ^{12}CO data for this region indicate (§ III*b*) gas temperatures significantly elevated, by a factor of 2 or more, above the 10 K which is characteristic (Dickman 1975) of most dark clouds (§ III*b*); simple theoretical considerations (Goldsmith and Langer 1978) suggest that this is due to the presence of embedded or nearby heating sources. The southeast filament of the ρ Oph cloud does, however, differ from the core in lacking the latter area's prolific star formation activity (Wilking and Lada 1983), as well as total mass (Loren 1989*a*).

b) Optical Star Count Data

The optical data for this paper are derived from deep prime focus plates of two $\sim 50'$—diameter areas obtained with the 4 m Cerro Tololo telescope. One region lies in the southeast filament of the cloud, L1689 (R.A. 1950 = 16^h30^m, decl. 1950 = $-24°30'$) and the other is a nearby, nearly extinction-free region (R.A. = $16^h32^m30^s$, decl. = $-25°00'00''$). Plates were exposed at the Kron J (4627 ± 487 Å), F (6167 ± 599 Å), and N (7941 ± 562 Å) bands (Bruzual 1966; Kron 1980) with a Racine prism, and densitometry of each plate was carried out on the Yale PDS. A more detailed description of this work is given elsewhere (Dickman and Herbst 1988; hereafter DH), and we summarize it here.

The plates were calibrated as follows. First, *BVRI* photoelectric photometry to $V \sim 17$ was obtained for a number of stars in the cloud and reference region with the single-channel photometer on the 60 inch (1.5 m) CTIO telescope. The *BVI* magnitudes were converted to their J, F, N equivalents using the transformations given by Fernie (1983). The resulting J, F, and N magnitudes for each star were then used to calibrate densitometric diameter-brightness sequences at each color in both fields. Because a Racine wedge was used for the 4 m photography (thus creating a secondary image of each star, fainter by ~ 6.9 mag than each primary image and displaced from it by some 30″), calibration of the fields was secured to the plate limit in each color. We estimate the accuracy of the magnitude determination in each band to be ~ 0.2 mag or better.

The end result of this process was a catalog containing the coordinates and J, F, N magnitudes of each star brighter than the plate limits in the cloud and reference fields. The reference field data and those for a nearly unobscured portion of the main cloud field were then used to construct sequences of cumulative star number surface densities at each color (DH).

Extinctions in the cloud relative to the reference field, A, at each color were initially determined at 98″ resolution using the method of cumulative star counts (Dickman 1978). With the rather conservative cut-off of $N \sim 20$ imposed in the N-band star counts (DH), the extinction in a single pixel containing no stars brighter than $N = 20$ is at least $A_N \sim 5.6$ mag. However, the presence of adjacent star-free pixels provides additional information on the mean extinction in such areas, and in the portion of the ρ Oph cloud studied here, the largest star-free areas have a minimum mean extinction of $A_N \sim 9$. We have adopted the conventional value of 3.1 for the ratio of total to selective extinction, and using the reddening curve of Savage and Mathis (1979), this implies that $A_v \cong 1.7\ A_N$. Consequently, the largest visual extinction probed by the star counts is ~ 15 mag.

c) Radio Observations

Radio observations of the $J = 1$–0 rotational transitions of both ^{12}CO and ^{13}CO were also carried out for the $40' \times 40'$ region studied by the star counts. The data were obtained with the 14 m radio telescope of Five College Radio Astronomy Observatory. The spectral resolution of the observations was 250 kHz (corresponding to 0.67 km s^{-1} in the case of the ^{13}CO line and to 0.65 km s^{-1} in the case of the common isotopic line), and the inner $31' \times 31'$ portion of the region was mapped completely in each species at 98″ (i.e., twice ^{13}CO beamwidth) spacing; additional rectangular areas also spaced by 98″ were

obtained over selected portions of remainder of the cloud area covered by the star counts. The ^{13}CO lines in this portion of the cloud have $\Delta v \sim 1$–2 km s^{-1}, with most line widths wider than 1.5 km s^{-1}. While the 250 kHz filter resolution was rather coarse to resolve fully, the lines of the rare species ^{13}CO integrated intensities (which are independent of spectral resolution) were used in computing the LTE column densities (Dickman 1975) in each pixel covered by the radio data. Further details of the observations are described elsewhere (DH).

d) *IRAS Data*

Co-added *IRAS* images of a 4° × 4° field centered at 16^{h}30^m, −24°30′ (the SE corner of the ρ Oph cloud) were obtained at a pixel spacing of 1′ × 1′ in all four *IRAS* bands. Despite the pixel size of these maps, it should be emphasized that their resolution in the longer wavelength bands is substantially lower than this; at 100 μm the effective angular resolution of the *IRAS* beam is ∼5′ (cross-scan) and 3′ (in-scan), for example. The large field size was chosen to provide sufficient room for background removal; the site of our program field is only a few degrees from the ecliptic plane, and zodiacal emission is thus a main contributor to the diffuse IR emission in this region, particularly in the 25 and 60 μm bands.

The simplest way to calibrate *IRAS* co-adds is to compare them with corresponding all-sky images (HCONs) which have an absolute (although somewhat imprecise) calibration. Given the rather small (<1 square degree) area of the radio and optical field, we chose a tilted plane to fit and remove the total zodiacal background emission. The points of the plane corresponding to the zero intensity level were chosen such that they lie in areas known to have minimal optical extinction (as seen from both the red POSS plates and our own deep sky plates). Once the plane was fitted to both the HCON and co-added images, the latter was calibrated from the former. After calibration, the field was narrowed to the 40′ × 40′ block to be studied. Finally, the data were smoothed to an effective resolution of 3′ × 5′. All remaining analysis presented here will be for this data set.

III. RESULTS

a) *Calculation of Infrared Properties of Cloud*

Dust opacities and color temperatures can be obtained from the *IRAS* intensities if we adopt the simplifying assumption that the IR emission in each pixel comes from a uniformly heated column of dust grains with a uniform mean size (the validity of this assumption is discussed in § IV). A λ^{-1} emissivity law is also assumed to pertain everywhere in the cloud, and we ignore for the moment the possibility that a significant fraction of the infrared intensity in any of the *IRAS* bands arises from line emission rather than continuum processes (e.g. Sellgren 1984; Leger and Puget 1984).

Figures 1*a* and 1*b* show maps of the background-adjusted 12 and 100 μm *IRAS* intensities over a region ∼1° square and roughly concentric with the optical and radio fields of the cloud. In Figure 2, a map of ^{13}CO column density (see § IIc) covering the center of the infrared field is also shown. The fact that the cloud's boundaries are clearly delineated by emission at *both* 12 μm ($hc/k\lambda \cong 1000$ K) and 100 μm ($hc/k\lambda \cong 100$ K) suggests strongly that the IR emission from the cloud can be modeled as arising from two physically distinct populations of dust grains. Accordingly, we initially separated the intensities in each pixel into (12 μm, 25 μm) and (60 μm, 100 μm) pairs, each of which was used to compute a color temperature and optical depth; in doing this, the intensity ratios were subjected to the appropriate calibration and color corrections described by Beichman *et al.* (1984), as given in the *IPAC User's Guide* (1986).

For reasons which can be anticipated and which are in any case made obvious below, we shall refer to the color temperatures and opacities of the dust associated with the (12 μm, 25 μm) and (60 μm, 100 μm) emission pairs as pertaining to populations of "warm" and "cool" dust grains, respectively. It should be noted that while in principle the color temperatures and opacities of the two grain populations defined by the separation procedure may be extracted by a self-consistent, four-parameter fit to the four-band emission in each pixel, the treatment based on splitting the *IRAS* emission into two subsets is numerically more stable, particularly at the edges of the cloud. Ex post facto checks of the results obtained by this method, made by correcting the emission in each emission pair set for contamination by the other set, and then re-computing color temperatures and optical depths, yielded results that in most cases were unchanged within 5%; in the worst cases (several pixels in the vicinity of a few bright point sources, where a simple model of grain emission cannot, in any case, be relied upon), corrections to the optical depth as large as 20% were found.

Figures 3*a* and 3*b* show in contour form the color temperatures of the warm and cool dust populations, respectively. Figures 4*a* and 4*b* are gray-scale representations of the opacities associated with these two grain populations; in Figure 4*b*, the 60 μm opacity map has also been overlaid with smoothed contours of ^{13}CO column density.

b) *Dust Color Temperature, Gas Kinetic Temperature, and Optical Depth*

Color temperatures computed from the long-wavelength emission pair (60/100 μm), vary from 20 to 40 K (see Fig. 3*b*), with temperatures in the central region of the cloud typically 25–30 K. Peaks of 35 K occur toward two bright point sources, *IRAS* 16293−2424 and 16293−2422, but care must be taken in interpreting this value, as a steep dust temperature gradient along the line of sight would be expected toward a bright point source embedded in the cloud, invalidating the simple homogeneous model adopted here.

Away from the central regions of the cloud field (the cloud edge is the extreme southern region of the box; see Fig. 2) the color temperature of the dust emitting at 60 μm and 100 μm smoothly rises from 25 K to a maximum of ∼40 K. This implies that the homogeneous model adopted to characterize the dust is invalid. Because the dust emission is weighted by temperature in an essentially exponential fashion, the temperature of the emitting material must in fact possess a much steeper line of sight gradient than the projected center to edge variation exhibited by the simple color temperature estimator adopted here. In any case, the limb brightening is probably due to external radiation penetrating the surface of the cloud, a fact predicted theoretically by Spencer and Leung (1978) for dark globules of $A_v > 10$, and discussed further in § IV.

In contrast to the results above, Green and Young (1989) claim that for the central core region of ρ Oph, the ISRF plays less an important role in heating the dust as compared to the total contribution provided by embedded luminous members of the core. The L1689 region has few sources that emit enough

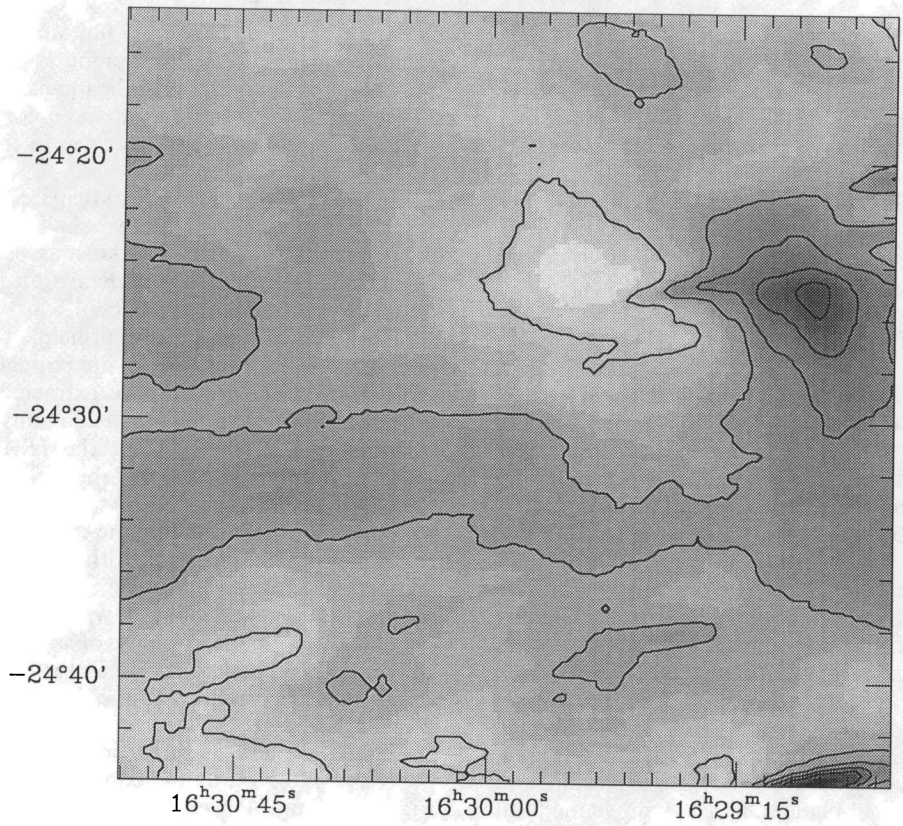

FIG. 1*a*

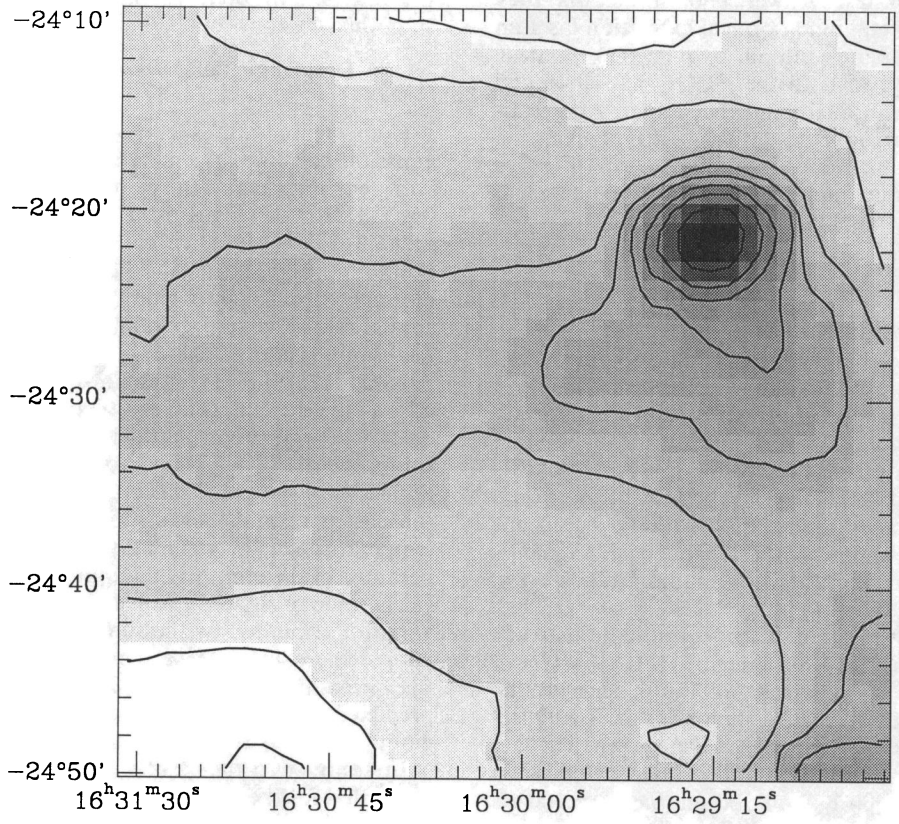

FIG. 1*b*

FIG. 1.—Co-added *IRAS* intensity images of a 40′ × 40′ field centered at (16h30s, 24°30′), shown for two of the *IRAS* bands. Contour levels in units of the median noise for each band, are as follows: (*a*) 12 μm: ($\langle n \rangle = 8.83 \times 10^4$ Jy sr^{-1}); 30, 45, 60, 75, and 90. (*b*) 100 μm: ($\langle n \rangle = 1.50 \times 10^6$ Jy sr^{-1}); 1, 10, 25, 50, 75, 100, 150, and 200, 300, and 400.

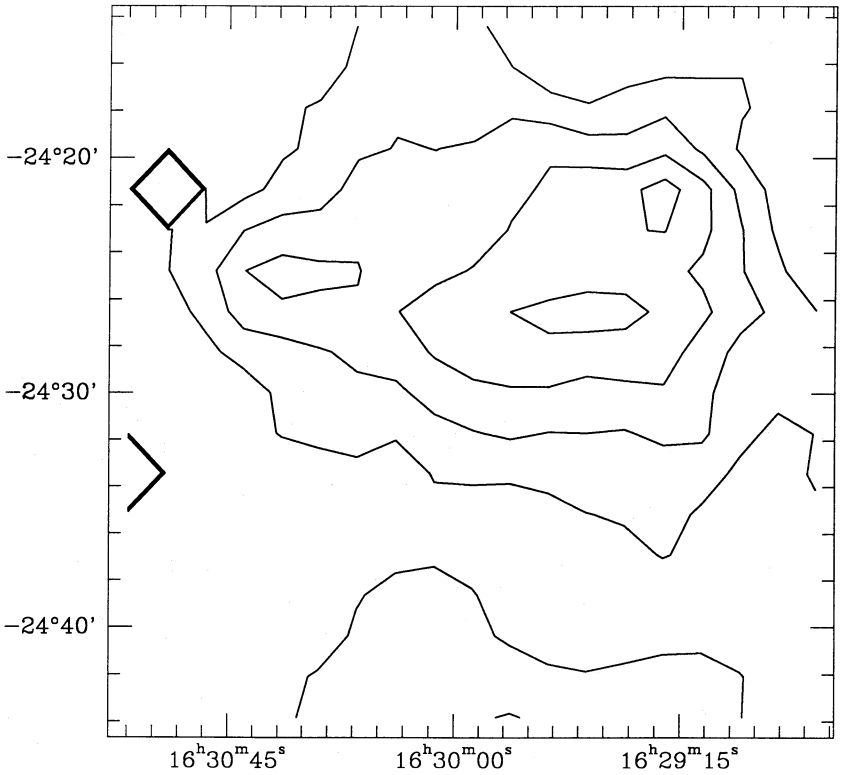

FIG. 2.—The ^{13}CO column density; N_{13} ($\times 10^{15}$ cm^{-2}) contours are 7, 10, 13, and 16

radiation to elevate dust temperatures to levels detectable by *IRAS*, thereby leaving the ISRF (which is appreciable due to the OB association) as the dominant-heating component. In this respect, the L1689 region is more similar to the cool Taurus clouds than to the star-forming core of the ρ Oph complex.

The (60/100 μm) color temperature, T_c versus $J = 1$–0 ^{12}CO radiation temperature at only those locations where ^{13}CO was detected is shown in Figure 5. Since the CO must be optically thick at these points, the radiation temperature is related to the gas kinetic temperature by $T_{kin} \cong T_{rad} + 3.4$ K if the molecular gas has a uniform excitation temperature (the last term represents the Rayleigh-Jeans contribution of the 2.7 K cosmic background). Nearly all the points lie in the temperature range

$$25 \leq T_c \leq 32 \quad \text{and} \quad 12 \leq T_{rad} \leq 20 ,$$

with T_c typically exceeding T_{kin} by 10 K. Because of the exponential weighting of the IR emission with dust temperature, as well as the edge heating of the cloud noted above, it would be simplistic and risky to conclude that these results indicate that the dust is everywhere warmer than the gas by some 10 K. However, the reasonably small scatter reflected by most of the data in Figure 5 does suggest that over much of the cloud region which we studied, dust and gas temperatures are coupled fairly closely. An exception are the few points with a higher color temperature (>32 K) and a lower radiation temperature (<12 K). These lie near the southern edge of the cloud. If one assumes that the positive center to edge color temperature gradient reflects the presence of a similar gradient in the gas and dust in the cloud, the radiation temperature of the molecular gas at these positions *does not* accurately estimate the gas kinetic temperature. Presumably, this is because the gas density at these locations is too low to maintain the CO in LTE, as well as to maintain gas-dust coupling.

In contrast to these results, short wavelength (12/25 μm) color temperatures vary from 200 to 290 K, as shown in Figure 3*a*. While there is a "hole" in the NW corner ($T \sim 200$ K), undoubtedly an artifact produced by the breakdown of our simple dust model near the point source *IRAS* 16293−2424, the short-wavelength color temperatures are for the most part remarkably uniform and lie in the range 230–270 K.

If the color temperature inferred from the 60 and 100 μm emission is physically meaningful there should be *no* 12 and 25 μm emission from the cloud at all. Likewise, the color temperature calculated from the short-wavelength emission is far too high to be attributed to "normal" dust intermixed with the cloud gas and suggests a distinct population of small dust grains (see Sellgren 1984) with its own excitation mechanism. We discuss this issue further in § IV.

The 60 μm optical depth (τ_{60}) associated with the cool grains varies from 10^{-2} to 10^{-6} (Fig. 4*b*). Typical values inside the cloud are 10^{-4}, with the dense clump in the NW region, having $\tau_{60} \sim 10^{-2}$. As one moves outward from the central cloud region, τ_{60} decreases by more than 2 orders of magnitude and shows an anticorrelation with the corresponding color temperature (see § IV*a*). Overall, the cloud structure revealed in the 60 μm opacity map is very nonuniform, with local gradients and clumps. As discussed below, this nonuniformity is, for the most part, identifiable with the physical structure of the cloud.

The 12 μm optical depth (τ_{12}) corresponding to the "hot" grains (~250 K) is dramatically different from its long wavelength counterpart. It varies only by one order of magnitude, from $\sim 10^{-8}$ to 10^{-7} (Fig. 4*a*). Further, τ_{12} appears quite

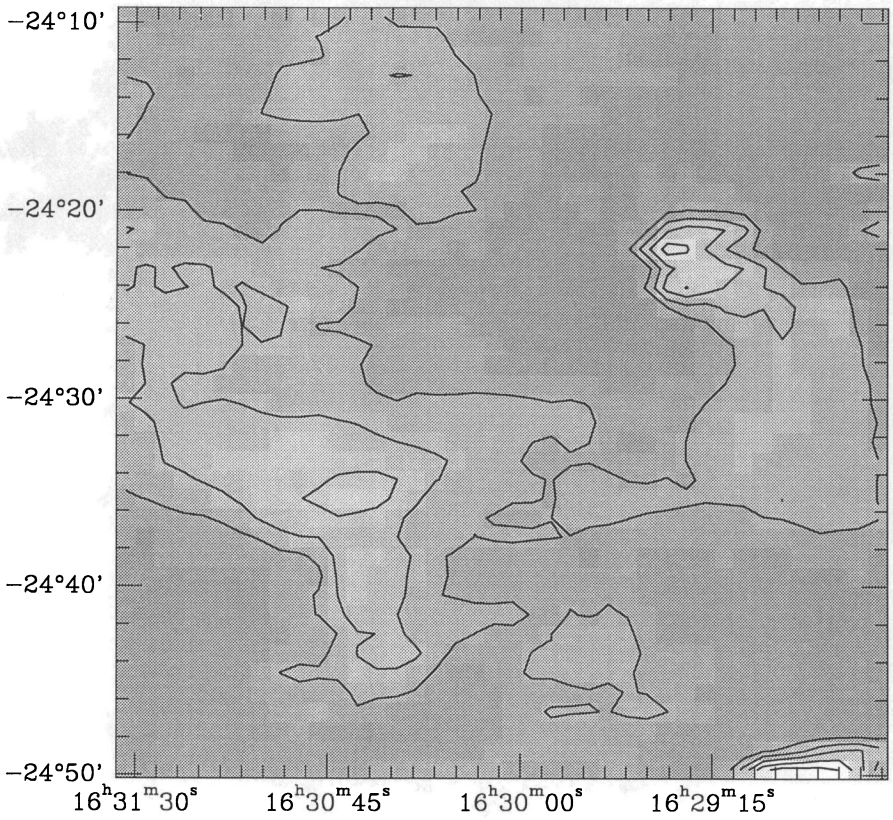

FIG. 3a

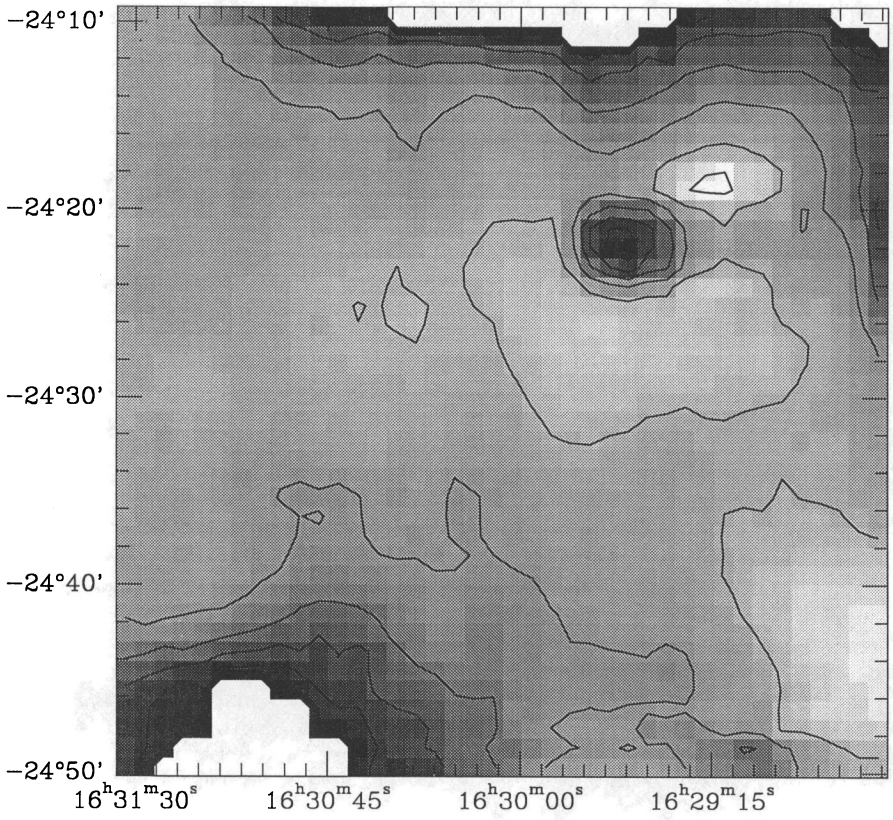

FIG. 3b

FIG. 3.—(*a*) Color temperature of 12 and 25 μm emission, using a λ^{-1} emissivity law. Temperature contours and gray-scale values: T(K) = 200, 220, 240, 260, and 280. (*b*) Color temperature of 60 and 100 μm emission, using a λ^{-1} emissivity law. Temperature contours and gray-scale values: T(K) = 22, 25, 28, 31, 34, and 37.

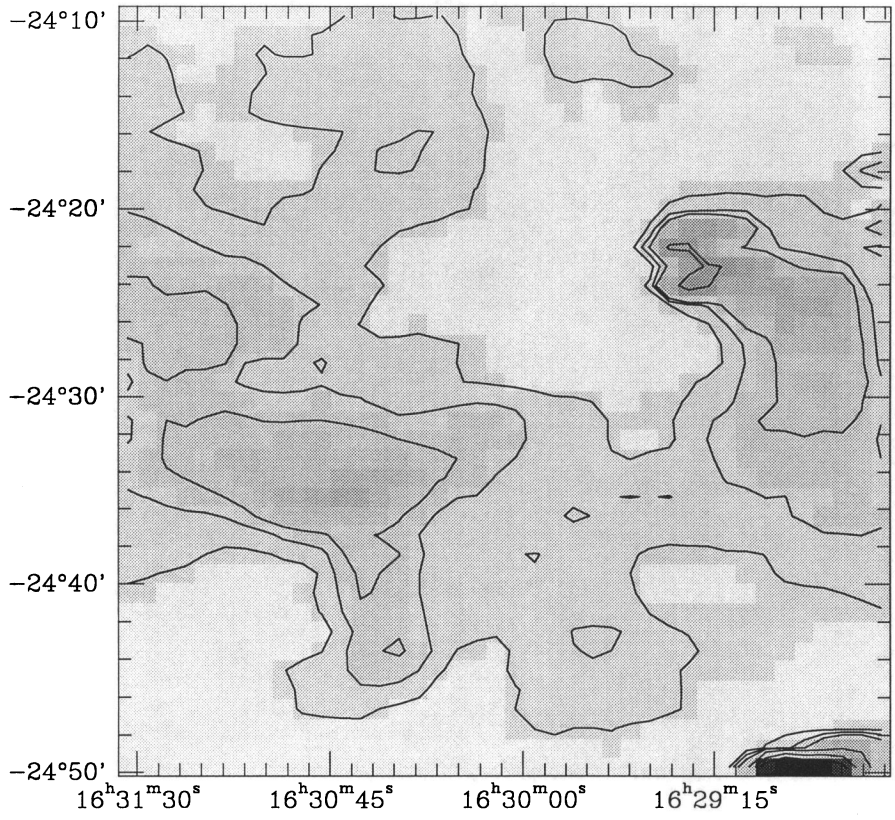

FIG. 4a

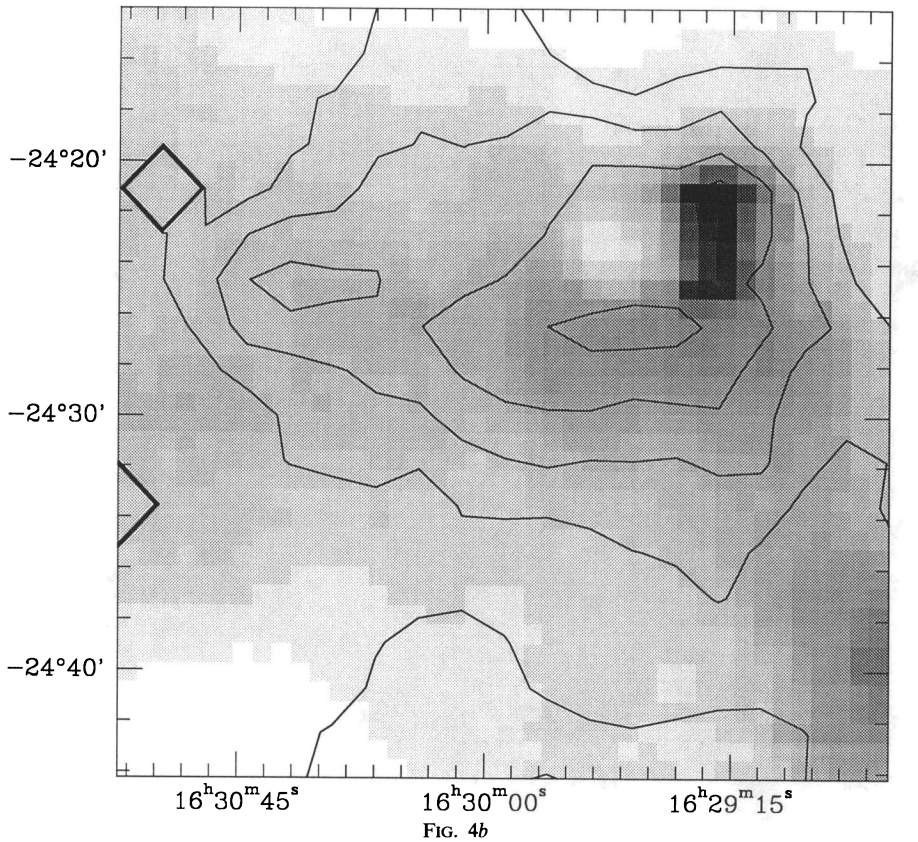

FIG. 4b

FIG. 4.—(*a*) 12 μm dust opacity, computed from the 12 μm intensity image and the corresponding color temperature image (Fig. 3*a*). The contour levels are in units of 10^{-8} and are 1, 1.5, 2, 5, 10, and 15. (*b*) 60 μm dust opacity, computed from the 60 μm intensity image and the corresponding color temperature image (Fig. 3*b*). The gray-scale ranges from 10^{-5} to 8×10^{-3}. Overlaying the dust opacity are smoothed contours of ^{13}CO column density, N_{13}, at levels 7, 10, 13, and 16×10^{15} cm.

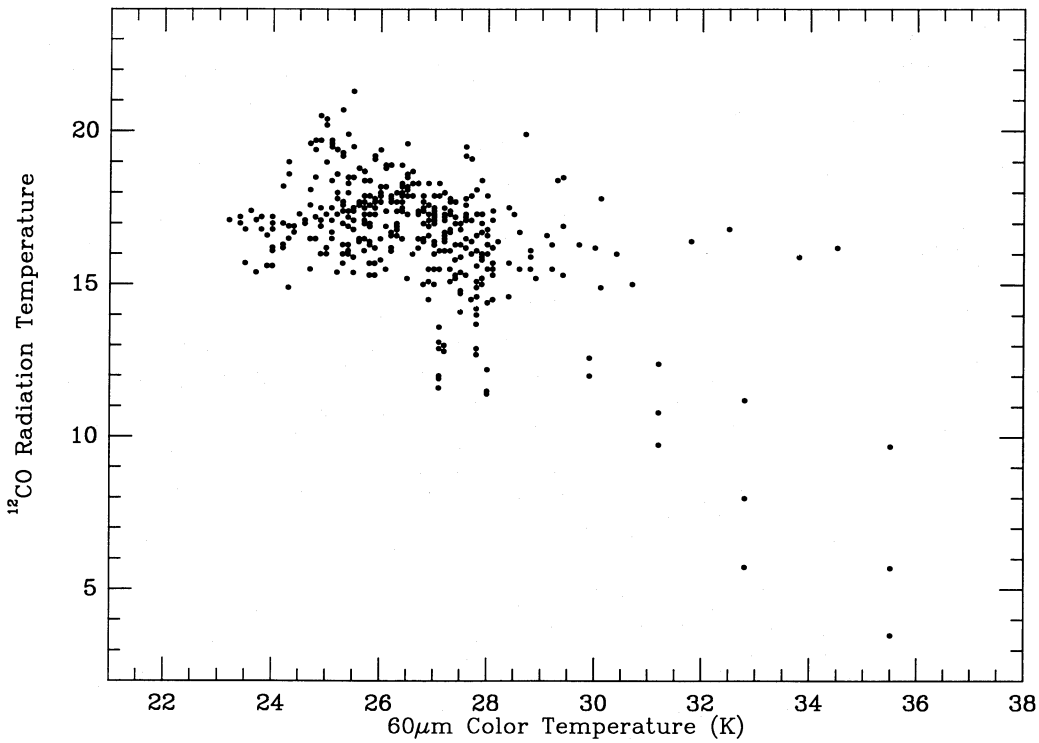

FIG. 5.—The (60/100 μm) color temperature vs. $J = 1$–0 ^{12}CO radiation temperature. Since the CO is optically thick, the latter quantity is related to the gas kinetic temperature by $T_{kin} \cong T_{rad} + 3.4$ K.

uniform throughout the bulk of the cloud, suggesting that the small grains emitting at 12 and 25 μm are poorly correlated with their larger counterparts. This is clearly seen in Figure 6, where we compare the two optical depth measures τ_{12} and τ_{60} point by point. Given the low dynamic range exhibited by τ_{12} over the cloud, this argues that the grain population responsible for the 12 and 25 μm emission is either absent or unheated over much of the cloud. This fact along with the presence of significant line emission in the short-wavelength *IRAS* bands probably renders the 12 and 25 μm emission unreliable in tracing the interior structure of molecular clouds (see Leger and Puget 1984; Puget, Leger, and Boulanger 1985). This point is discussed further in § IV.

c) *Dust and Gas/Extinction Comparison*

In Figure 7 is a plot of 12 μm optical depth versus the visual extinction in each map pixel derived from the N-band star counts. The striking absence of a perceptible correlation between these two quantities illustrate directly that the 12 μm opacity does not trace well the interior structure of the cloud. In contrast, the 60 μm opacity determined from the long-wavelength *IRAS* data does appear to trace both the dust column density revealed by the star counts as well as the ^{13}CO gas column density. This seen in Figure 8 where we plot τ_{60} versus A_v, the visual extinction difference between the cloud and reference field, determined from star counts at the Kron N-band (§ II*a*). Up to $A_v \sim 5$ mag, there is a tight correlation between the two quantities which follows the roughly linear relation:

$$A_v \cong 1.2 \times 10^4 \, \tau_{60} \, . \qquad (1)$$

Beyond $A_v \sim 5$ mag the scatter increases dramatically.

Similarly, in Figure 9 we plot τ_{60} versus ^{13}CO LTE column density. As in the previous instance, at small optical depths, $\tau_{60} \leq 10^{-4}$, and correspondingly low column densities ($N_{13} < 10^{16}$ cm^{-2}), the gas and dust correlate well. A linear fit to these two quantities (also shown on the plot) yields:

$$N_{13}(10^{15} \text{ cm}^{-2}) \cong 1.9 \times 10^4 \, \tau_{60} \, . \qquad (2)$$

As in the case of the τ_{60} versus A_v plot, considerable scatter is seen at higher optical depths and column densities although the trend quantified above continues to $\tau_{60} \sim 10^{-3}$. We discuss the significance of the greatly increased scatter associated with τ_{60} at high visual extinctions and ^{13}CO column densities in § IV.

d) *Mass of the Dust and Gas*

For a line of sight with a column density N_g of identical grains having a radius a, the mass column density can be written (Hildebrand 1983),

$$\sigma_d \text{ (g cm}^{-2}) = (\tfrac{4}{3})[a\rho/Q]\tau_{60} \qquad (3)$$

where ρ is the grain density and Q is the emission efficiency at 60 μm; this formula is a trivial extension of the fact that $\tau_\lambda \cong \pi\langle a^2\rangle Q_\lambda N_{gr}$. Using Hildebrand's (1983) average value for $[Q/a\rho]$ of 3.2 (1000/λ μm), for a mixture of silicate and graphite grains, we obtain at 60 μm:

$$\sigma_d \text{ (g cm}^{-2}) = 2.5 \times 10^{-2} \, \tau_{60} \qquad (4)$$

We can compute the ratio of gas to dust mass column density using

$$\sigma_{gas}/\sigma_d = N_{H2} \, m_{H2}/2.5 \times 10^{-2} \qquad (5)$$

Using Bohlin, Savage, and Drake's (1978) value for the relation between gas column density and visual extinction, $N_{H2} \cong 10^{21} A_v$, and the slope of the extinction to 60 μm opacity correl-

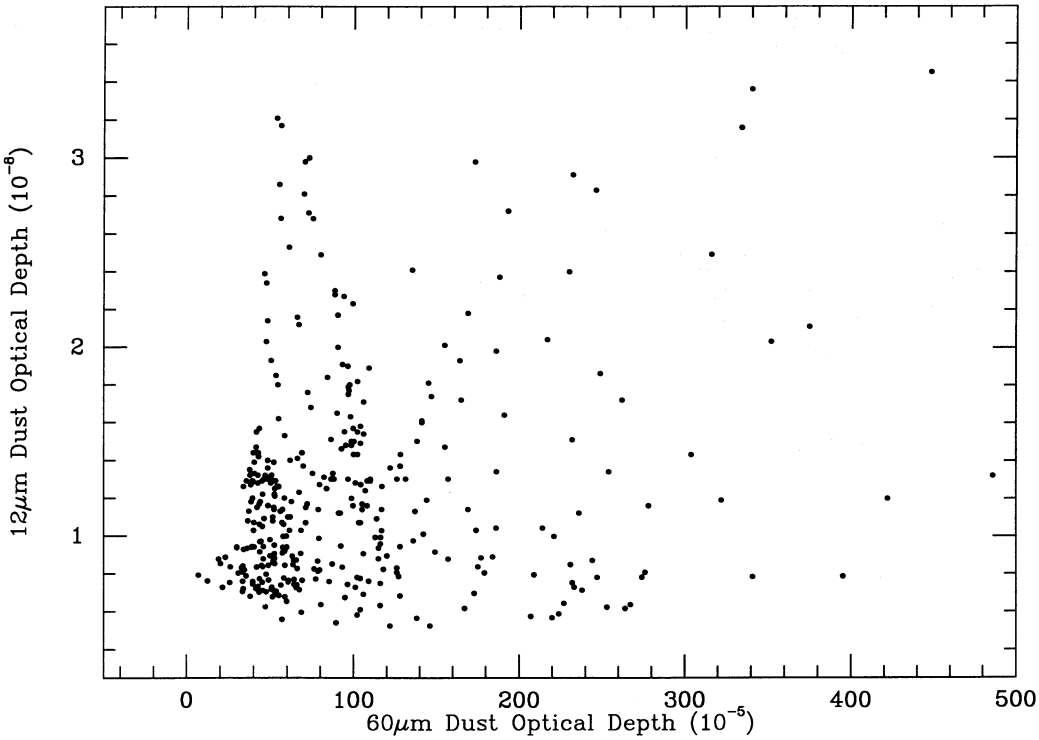

FIG. 6.—60 μm vs. 12 μm optical depth, plotted pixel by pixel from Figs. 4*a* and 4*b*

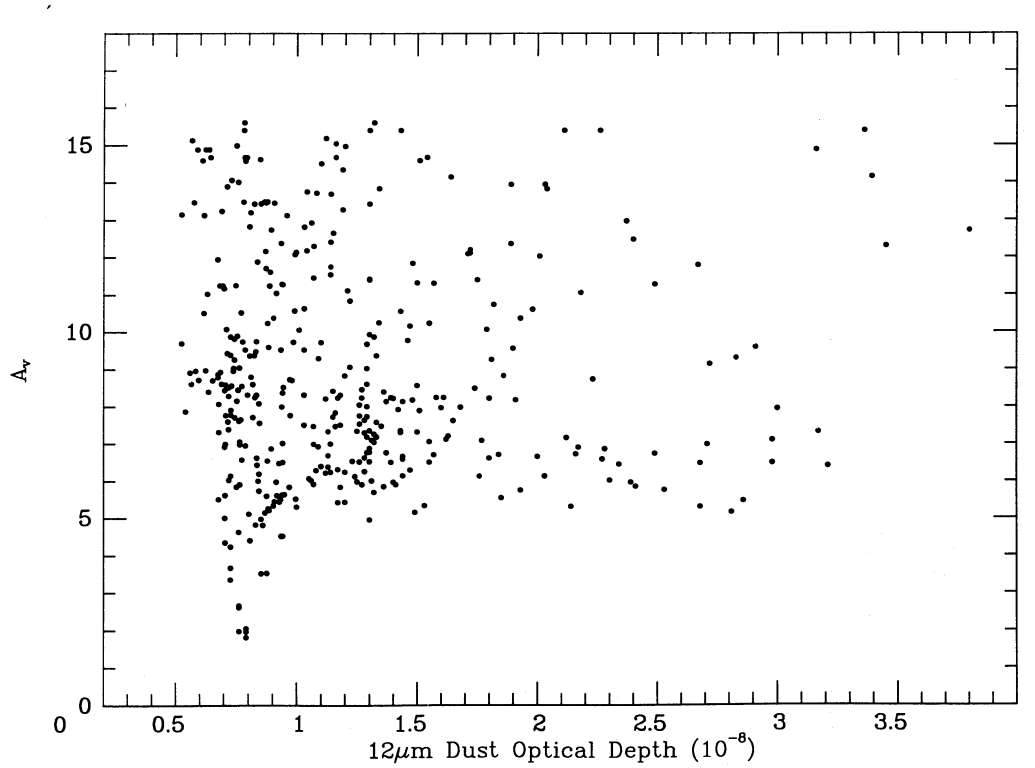

FIG. 7.—12 μm optical depth vs. visual extinction, A_v, determined from calibrated star counts at Kron N-band ($\lambda \sim 8000$ Å)

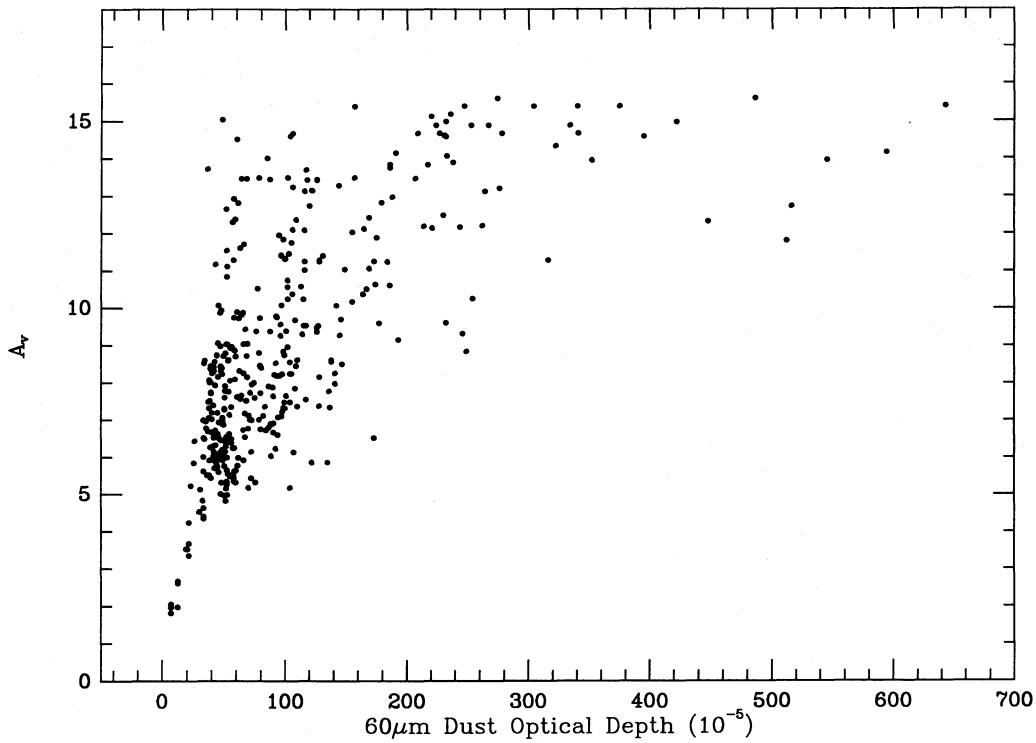

FIG. 8.—60 μm optical depth vs. visual extinction, A_v, determined from calibrated star counts at Kron N-band ($\lambda \sim 8000$ Å)

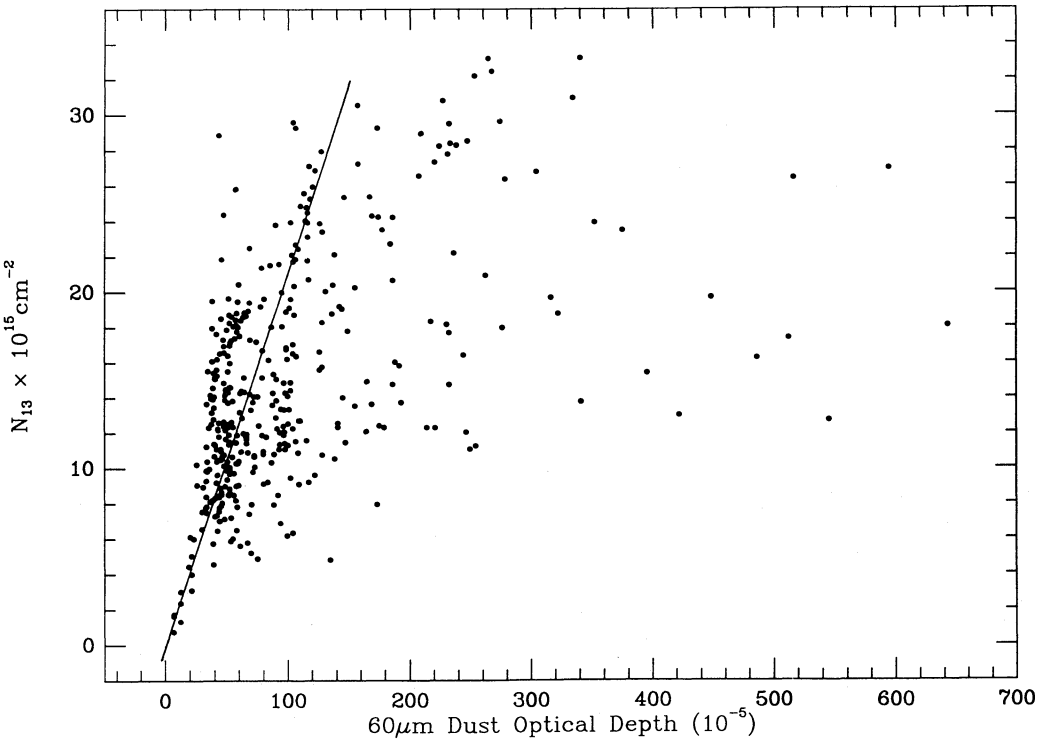

FIG. 9.—60 μm optical depth vs. ^{13}CO LTE column density expressed in units of 10^{15} cm^{-2}. Also shown is the linear fit: N_{13} (10^{15} cm^{-2}) $\cong 1.9 \times 10^4 \tau_{60}$

ation for low values of A_v, $A_v \cong 1.2 \times 10^4\ \tau_{60}$, we then find,

$$\sigma_{\rm gas}/\sigma_d = 1920\tau_{60} \quad (6)$$

Assuming a true gas to dust mass ratio of 100 (Hildebrand 1983), we conclude that only ~5% of the dust is visible at 60 and 100 μm. This result is consistent with those found by several other groups in their study of molecular clouds (e.g., Snell *et al.*, 1989; Langer *et al.*, 1988).

e) *Far-Infrared Luminosity*

In order to calculate the FIR luminosity of the portion of the cloud we have observed, we apply bolometric corrections of 2.7 and 2.8 to account for out of band emission stemming from the cool and warm grain populations, respectively; this assumes mean temperatures of 25 K and 250 K. The resultant integrated point by point luminosity for our field is then

$$L(\text{"cool" grains}) = 329\ L_\odot \quad (7a)$$

$$L(\text{"warm" grains}) = 198\ L_\odot \quad (7b)$$

giving a total of 527 $L_\odot$.

Summing the H_2 column density in each pixel (§ III*d*) gives a mass $M_{H2} = 587\ M_\odot$, assuming a distance of 160 pc to the cloud. The resulting IR luminosity to mass ratio is 0.9; this is significantly less than the mean value associated with the Galactic disk, but is significantly higher than that obtained by Snell *et al.* (1989) for the Taurus region, even if one considers the "cool" grain population alone. Presumably this reflects the more energetic environment of the upper Scorpius region (which produces more vigorous heating by the interstellar radiation field), as well as an internal cloud gas temperature (however poorly coupled to the dust) more than twice as high as the Taurus clouds.

IV. DISCUSSION

The results described above are consistent in several respects with those obtained by other groups studying the relationship between molecular cloud properties and *IRAS* emission. We have used a simple (and—as noted above—simplistic) uniform dust excitation model to derive opacities and color temperatures for the dust emitting at 60 and 100 μm. The variation of the color temperature with position in the cloud clearly requires the presence of an external dust heating mechanism capable of penetrating the Ophiuchus cloud to a reasonable depth (although there may be other heating mechanisms present as well). Further, as has been stressed before (Boulanger and Perault 1988; Langer *et al.* 1988; Snell *et al.* 1989), the fact that the opacities obtained in the 60 and 100 μm *IRAS* bands with the model imply a grossly incorrect gas to dust mass ratio, demonstrates that only a small fraction (~5%) of the dust is hot enough to produce the observed 60 and 100 μm emission. Despite this result (which is exacerbated by the exponential weighting of the hottest dust grains in the emission process) a reasonably linear correlation between IR opacity and ^{13}CO column density exists in the cloud up to a threshold $N_{13} \sim 10^{16}$ cm^{-2}. A similar correlation is found between IR opacity and visual extinction up to a limit of ~5–6 magnitudes. Within a factor of 2 or so, the slope of this relation is the same as that in the Taurus (Snell *et al.* 1989) and Perseus (Langer *et al.* 1988) regions. Thus, in three very different environments 60 and 100 μm dust emission is empirically found to constitute a good tracer of molecular cloud mass, up to dust column densities which correspond to extinctions in the visual of 5–6 mag.

The entire ρ Ophiuchi cloud is clearly visible at both 12 and 25 μm. This is not an uncommon situation for warm molecular clouds. Both the Orion (Boulanger and Perault 1988) and Perseus (Beichmann *et al.* 1988) clouds, for example, are readily apparent in all *IRAS* bands. However, in the area of the ρ Oph cloud under study in this work, neither the short-wavelength IR intensities nor the opacities which can be derived from them show a significant positional correlation with the mass tracers A_v, τ_{60}, and N_{13}. The limited dynamic range (roughly order of magnitude) of the τ_{12} values, and the unrealistically high color temperatures deduced from the 12 and 25 μm intensities of the cloud material suggest heating by an easily attenuated (and thus presumably short-wavelength) external radiation source. A similar conclusion concerning the excitation source of the 12 and 25 μm radiation seen in Barnard 5 was reached by Beichmann *et al.* from analysis of the edge-brightening of the short-wavelength IR emission.

If this interpretation is correct, the association of warm molecular clouds with high levels of 12 and 25 μm emission does not reflect a direct causal relationship. The clouds are not bright at the shorter IR wavelengths because they happen to be warm; rather, the same factor which leads to the heating of molecular material above the ~10 K typical of dark clouds—namely, massive star formation—leads both to the production of a sufficient number of grains (or PAH-like particles; e.g., Leger and Puget 1984) small enough to sustain the high-temperature excursions required for emission at 12 and 25 μm, and to a radiation field rich in excitation photons.

A unique aspect of this study is the use of calibrated star counts deep enough to test quantitatively the validity of τ_{60} as a mass tracer at the very large extinction ($\gtrsim$6 mag) characteristic of giant molecular cloud cores. We have already noted in Figures 8 and 9 that τ_{60} follows both A_v and N_{13} up to thresholds of ~5–6 mag and 10^{16} cm^{-2}, respectively, and that beyond these points, the scatter in the correlations appears to increase substantially. This effect appears to be associated primarily with the IR measure. Both N_{13} and A_v correlate with each other in a reasonably linear fashion well above the scatter thresholds in Figures 8 and 9 (DH). While it is not completely impossible that a combination of factors is responsible for the persistence of this correlation beyond the point where either or both of these (independently determined) quantities reliably estimate the column densities of dust and gas, it seems more reasonable to attribute the breakdown in the correlations of Figures 8 and 9 to a problem with the 60 μm optical depth.

This does not necessarily imply that τ_{60} becomes useless as a dust column density measure above visual extinctions of 5 or 6 mag. The pixels with the largest 60 μm opacity scatter in Figures 8 and 9 are not randomly located in the cloud, but are, for the most part, centered about the unusual outflow source *IRAS* 16293−2422 (Walker *et al.* 1986, 1988), located at $\alpha = 16^h29^m20^s.9$, $\delta = -24°22'13''$. This source directly abuts the prominent 60 μm opacity core centered roughly at $\alpha = 16^h29^m12^s$, $\delta = -24°22'00''$, as well as the apparent 60 μm "hole" lying some 15^s to the East (see Fig. 4*b*).

In Figure 10 we have replotted the 60 μm visual extinction data using squares to identify pixels which lie in a ~10′ × 10′ square region centered on *IRAS* 16293−2422. Clearly, the τ_{60}–A_v correlation is greatly improved when locations near the outflow source are excluded; the best-fit straight line to the remaining data points (restricted to values of $A_v < 9.5$ mag in

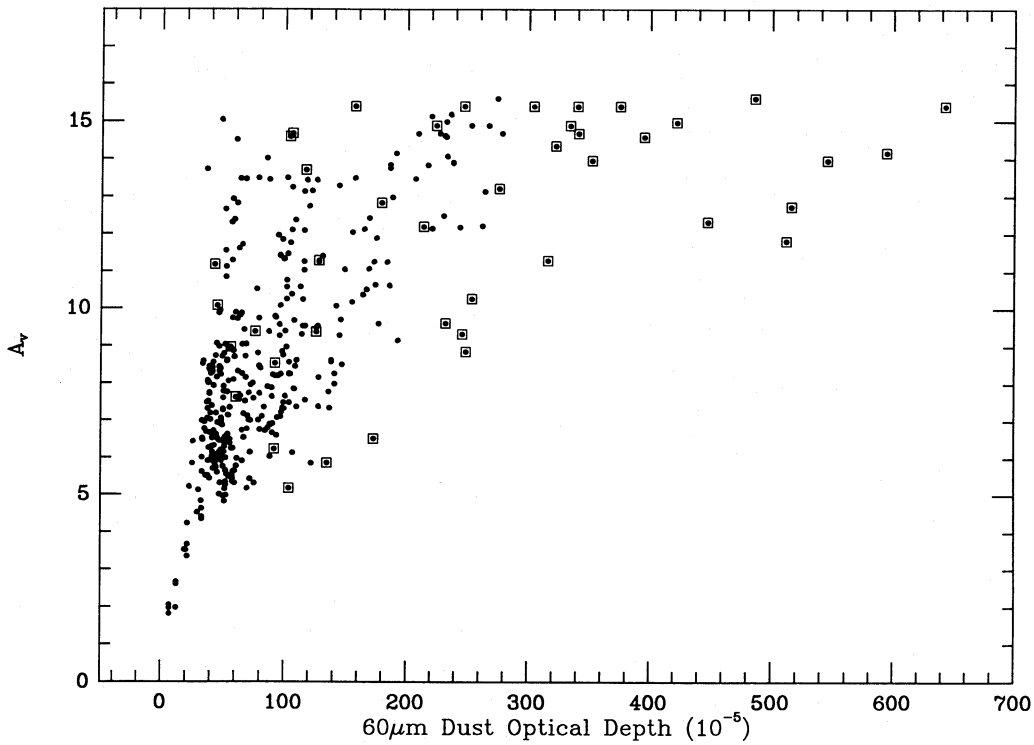

FIG. 10.—60 μm optical depth vs. ^{13}CO LTE column density, replotted using squares to identify pixels which lie in a 10′ × 10′ square region centered on *IRAS* 16293 − 2422, located at $\alpha = 16^h29^m20^s.9$, $\delta = -24°22'13''$.

order to avoid including lower limits to the extinction) is

$$A_v = 6700 \times \tau_{60} + 2.1 \quad (8)$$

The scatter of the data about this linear relation is quantitatively similar to that found by Snell, Heyer, and Schloerb (1989) for the Taurus dark clouds. (There is a slight suggestion in the remaining data of a rather abrupt increase in scatter above $A_v \sim 5$–6 mag, but it is difficult to be certain that this is not due mainly to the fact that the visual extinction values themselves become progressively more uncertain at higher values of A_v. In addition, one would expect scatter due to the diminishing number of exciting photons at large column densities; as posed in § III, the 60 μm optical depth appears to be derived from a surface layer of cool-grain emission, thus at higher densities the measure is less likely to reflect the true grain column density).

The 60 μm opacities excluded from the fit above are generally larger than those elsewhere in the cloud, and also appear to be characterized by enhanced scatter (although the fact that the largest visual extinctions shown in Figure 10 are lower limits should be kept in mind). What is the cause of this behavior? *IRAS* 16293 − 2422 must heat the dust in its vicinity, probably both directly, and via its associated outflow. This zone of influence, as traced by the CO $J = (2–1)$ observations of Walker *et al.* (1988), extends *at least* as far as 2′ from the driving source, and is almost certainly larger. Given the exponential sensitivity of the 60 and 100 μm emission to small changes in dust temperature, along with the fact that the vast majority of the dust in the Oph cloud is evidently too cold to emit within the long-wave *IRAS* bands (§ III*d*), even a slight (< 5 K) elevation in the temperature of a small quantity of dust near the outflow source would lead to greatly enhanced IR emission at both 60 and 100 μm, invalidating the simple opacity model used to analyze the IR data and leading to an overestimate of the dust's optical depth.

The $J = (2–1)$ CO observations of Walker *et al.* 1988 also reveal the cloud material perturbed by the outflow to be strongly clumped. This clumpiness may originate in a variety of dynamical instabilities at the boundary between the cavity evacuated by the stellar outflow itself and the neutral, ambient molecular cloud (Moriarty-Schieven *et al.* 1987), and may be superposed upon an already fragmentary internal cloud structure stemming from a strongly turbulent velocity field (Dickman 1985; Taylor and Dickman 1989). Although we have not attempted a detailed model, it seems likely that the transport of heating photons to the ambient dust from the central star and the outflow/cloud interface will be strongly randomized by the clumped material in the outflow's vicinity. This would then account for the large scatter in the 60 μm optical depth which is seen in Figure 10 in the region surrounding *IRAS* 16293 − 2422.

These factors suggest that in order to successfully exploit the full dynamic range of the *IRAS* data base to probe molecular clouds, it will probably be necessary to avoid areas near outflow sources. One can expect that these areas will often be considerably larger in *spatial* extent than the core region treated above: the pixels excluded from the fit in equation (8) extend out to ~0.25 pc from the perturbing outflow source. *IRAS* 16293 − 2422 has an IR luminosity $L \sim 23\ L_\odot$, not an especially large value. By contrast, most of the AFGL objects recently studied by Snell *et al.* (1988), which are among the most luminous outflow sources, have luminosities 1000 times larger than this, and might therefore be expected to invalidate simple IR column density measures over much larger regions than is the case here. Fortunately, such objects are rare, and at least in the case of the best-studied GMCs, reasonably com-

plete tallies of outflow sources (Lada 1985; Snell 1987) are beginning to emerge. Such lists can help to identify potentially troublesome regions insofar as application of the *IRAS* data base is concerned, although bias-free outflow surveys (e.g., Margulis 1987; Snell *et al.* 1988) are really needed for this purpose.

With this caveat, the correlation given in relation (8) indicates that even a simplistic two-color treatment of *IRAS* 60 and 100 μm intensity data can yield values for the infrared opacity which are well correlated with visual extinction, even at $A_v \geq 10$ mag. Only a very small fraction of the angular area of even the closest massive molecular clouds possess extinctions so large; indeed, Lynds (1962) found that only ~0.3% of all obscuring matter visible from the northern hemisphere possesses an extinction of 6 mag or greater. Although it is unclear whether visual extinction itself traces the gas content of molecular clouds in a purely linear fashion at high A_v (Dickman 1988; DH), relation (8) indicates that, in principle, the *IRAS* data is capable of *quantitatively* tracing the vast majority of the interstellar dust within our Galaxy.

V. CONCLUSIONS

Data from the *IRAS* satellite reveal the ρ Ophiuchi molecular cloud to be clearly visible at 12 and 25 μm, as well as at 60 and 100 μm.

Modeling the infrared emission from the cloud as being due to two populations of dust grains, we find the short-wavelength emission does not reflect the internal structure of the molecular cloud. We suggest this emission is a surface phenomenon.

The 60 μm opacity determined using a simple grain emission model correlates reasonably well with ^{13}CO column density and visual extinction up to $A_v \approx 5$ mag, a level significantly below the saturation points of both measures. Above this threshold, scatter in the 60 μm opacity is much larger. This effect is due primarily to the influence of an embedded outflow source in the center of the region studied. When data in the vicinity of the source are excluded, the simple 60 μm opacity is found to correlate well with extinction even up to $A_v \geq 10$ mag. This suggests that the *IRAS* data base can in fact be used to trace most of the dust within the Galaxy.

The cloud edges appear to be heated by the interstellar radiation field. At the extreme edges of the cloud, there is evidence that the ^{12}CO $J = 1 \rightarrow 0$ emission is not thermalized, even at locations where ^{13}CO remains detectable.

Finally, we determine the far-infrared luminosity to mass ratio for this region to be 0.9 $L_\odot/M_\odot$, a value slightly higher than what is observed in other dark clouds, yet is still much smaller than the average ratio for the inner Galaxy.

This research was supported in part by a NASA *IRAS* guest investigator grant and in part by NSF grant 85-12903 to Five College Radio Astronomy Observatory. We thank Carolyn Jordan for her contributions to this program in its early stages. This is contribution No. 668 of the Five College Astronomy Department.

REFERENCES

Beichman, C. A., Neugebauer, G., Habing, H. J., Clegg, P. E., and Chester, T. J. 1986, *IRAS Expanatory Supplement* (Washington, DC: US GPO).
Beichman, C. A., Wilson, R. W., Langer, W. D., and Goldsmith, P. F. 1988, preprint.
Beichman, C. A., *et al.* 1984, *Ap. J. (Letters)*, **278**, L45.
Bohlin, R. C., Savage, B. D., and Drake, J. F. 1978, *Ap. J.*, **224**, 132.
Bok, B. J. 1956, *A.J.*, **61**, 309.
Boulanger, F., and Perault, M. 1988, *Ap. J.*, **330**, 964.
Brown, R. L., and Zuckerman, B. 1975, *Ap. J.*, **264**, 134.
Bruzual, G. A. 1966, Ph.D. thesis, University of California, Berkeley.
Carrasco, L., Strom, S. E., and Strom, K. M. 1973, *Ap. J.*, **182**, 95.
Cernicharo, J., and Guélin, M. 1987, *Astr. Ap.*, **176**, 299.
Dickman, R. L. 1985, in *Protostars and Planets II*, ed. D. C. Black and M. S. Mathews (Tucson: University of Arizona Press), p. 150.
———. 1975, *Ap. J.*, **202**, 50.
———. 1978, *A.J.*, **83**, 363.
———. 1988, in *Molecular Clouds in the Milky Way and External Galaxies*, ed. R. L. Dickman, R. L. Snell, and J. S. Young (Berlin: Springer-Verlag), p. 55.
Dickman, R. L., and Herbst, W. 1989, in preparation.
Draine, B. T. 1985, in *Protostars and Planets II*, ed. by D. C. Black and M. S. Mathews (Tucson: University of Arizona Press), p. 621.
Elias, J. H. 1978, *Ap. J.*, **224**, 453.
Fernie, J. D. 1983, *Pub. A.S.P.*, **95**, 782.
Goldsmith, P. F. and Langer, W. D. 1978, *Ap. J.*, **222**, 881.
Grasdalen, G. L., Strom, K. M., and Strom, S. E. 1973, *Ap. J. (Letters)*, **184**, L53.
Green, T. P., and Young, E. T. 1989, *Ap. J.*, **339**, 258.
Herbst, W., and Warner, J. W. 1981, *A.J.*, **86**, 885.
Hildebrand, R. 1983, *Quart. J.R.A.S.*, **24**, 267.
Kron, R. G. 1980, *Ap. J. Suppl.*, **43**, 319.
Lada, C. J. 1985, *Ann. Rev. Astr. Ap.*, **23**, 267.
Lada, C. J., and Wilking, B. A. 1980, *Ap. J.*, **238**, 620.
Langer, W. D., Wilson, R. W., Goldsmith, P. F., and Beichman, C. A. 1988, preprint.
Leger, A., and Puget, J. L. 1984, *Astr. Ap.*, **137**, L5.
Loren, R. B. 1989*a*, *Ap. J.*, **338**, 902.
———. 1989*b*, *Ap. J.*, **338**, 925.
Loren, R. B., and Wootten, A. 1986, *Ap. J.*, **306**, 142.
Loren, R. B., Wootten, A., Sandqvist, A. A., and Bernes, C. 1980, *Ap. J. (Letters)*, **240**, L165.
Lynds, B. T. 1962, *Ap. J. Suppl.*, **64**, 1.
Margulis, M. 1987, Ph.D. thesis, University of Arizona.
Moriarty-Schieven, G. H., Strom, S. E., Schloerb, F. P., Strom, K. M., and Grasdalen, G. L. 1987, *Ap. J.*, **319**, 742.
Myers, P. C., Ho, P. T. P., Schneps, M. H., Chin, G., Pankonin, V., and Winnberg, A. 1978, *Ap. J.*, **220**, 864.
Puget, J. L., Leger, A., and Boulanger, F. 1985, *Astr. Ap.*, **142**, L19.
Savage, B. D., and Mathis, J. S. 1979, *Ann. Rev. Astr. Ap.*, **17**, 73.
Sellgren, K. 1984, *Ap. J.*, **277**, 623.
Snell, R. L. 1987, *IAU Symposium 115, Star Forming Regions*, ed. M. Peimbert and J. Jugaku (Dordrecht: Reidel), p. 213.
Snell, R. L., Heyer, M. H., and Schloerb, F. P. 1989, *Ap. J.*, **337**, 739.
Snell, R. L., Huang, Y. L., Dickman, R. L., and Claussen, M. J. 1988, *Ap. J.*, **325**, 742.
Spencer, R. G., and Leung, C. M. 1978, *Ap. J.*, **222**, 140.
Taylor, D., and Dickman, R. L. 1989, *Ap. J.*, **341**, 293.
Vrba, F. J., Strom, K. M., Strom, S. E., and Grasdalen, G. L. 1975, *Ap. J.*, **197**, 77.
Walker, C. K., Lada, C. J., Young, E. T., Maloney, P. R., and Wilking, B. A. 1986, *Ap. J. (Letters)*, **309**, L47.
Walker, C. K., Lada, C. J., Young, E. T., and Margulis, M. 1988, *Ap. J.*, **332**, 335.
Wilking, B. A., and Lada, C. J. 1983, *Ap. J.*, **274**, 698.
Wootten, A., and Loren, R. B. 1987, *Ap. J.*, **317**, 220.

R. L. DICKMAN and T. H. JARRETT: Five College Radio Astronomy Observatory, 619 Lederle Graduate Research Center, University of Massachusetts, Amherst, MA 01003

W. HERBST: Van Vleck Observatory, Department of Astronomy, Wesleyan University, Middletown, CT 06457